Connection between the packing efficiency of binary hard spheres and the glass-forming ability of bulk metallic glasses

Kai Zhang,[1,2] W. Wendell Smith,[3] Minglei Wang,[1,2] Yanhui Liu,[1,2] Jan Schroers,[1,2]
Mark D. Shattuck,[4,1] and Corey S. O'Hern[1,2,3,5]

[1]*Department of Mechanical Engineering and Materials Science, Yale University, New Haven, Connecticut 06520, USA*

[2]*Center for Research on Interface Structures and Phenomena, Yale University, New Haven, Connecticut 06520, USA*

[3]*Department of Physics, Yale University, New Haven, Connecticut 06520, USA*

[4]*Department of Physics and Benjamin Levich Institute, The City College of the City University of New York, New York, New York 10031, USA*

[5]*Department of Applied Physics, Yale University, New Haven, Connecticut 06520, USA*

We perform molecular dynamics simulations to compress binary hard spheres into jammed packings as a function of the compression rate R, size ratio α, and number fraction x_S of small particles to determine the connection between the glass-forming ability (GFA) and packing efficiency in bulk metallic glasses (BMGs). We define the GFA by measuring the critical compression rate R_c, below which jammed hard-sphere packings begin to form "random crystal" structures with defects. We find that for systems with $\alpha \gtrsim 0.8$ that do not demix, R_c decreases strongly with $\Delta\phi_J$, as $R_c \sim \exp(-1/\Delta\phi_J^2)$, where $\Delta\phi_J$ is the difference between the average packing fraction of the amorphous packings and random crystal structures at R_c. Systems with $\alpha \lesssim 0.8$ partially demix, which promotes crystallization, but we still find a strong correlation between R_c and $\Delta\phi_J$. We show that known metal-metal BMGs occur in the regions of the α and x_S parameter space with the lowest values of R_c for binary hard spheres. Our results emphasize that maximizing GFA in binary systems involves two competing effects: minimizing α to increase packing efficiency, while maximizing α to prevent demixing.

I. INTRODUCTION

Hard-sphere models provide quantitatively accurate descriptions of physical properties in systems where steric, repulsive interactions are dominant, such as the diverging viscosity near the glass transition in colloids [1], transport properties in simple liquids [2], and mechanical properties of granular materials [3]. For more complex materials with competing repulsive and attractive interactions, such as bulk metallic glasses, it is often helpful to develop a perturbative description where only hard-sphere interactions [4] are included to determine to what extent these alone can explain key physical properties [5,6].

Bulk metallic glasses (BMGs) are prepared by thermally quenching liquid alloys at sufficiently fast rates such that they bypass crystallization, and instead form amorphous solids [7,8]. Over the past 30 years, BMGs have been developed with optimized mechanical properties, such as enhanced strength and fracture toughness above that for steel [9], but with processing and molding capabilities similar to plastics [10]. However, their applications in industry are still often constrained by the high cost of the constituent elements and the maximum casting thickness of the material. The glass-forming ability (GFA) of a BMG is defined by the critical cooling rate below which the system begins to crystallize, which in turn determines its critical casting thickness [7]. An important open question is how to *de novo* design BMGs with desirable material properties and maximum glass formability by continuously varying the stoichiometry of the constituent elements [11].

There are well-known empirical rules for improving the glass-forming ability of BMGs, for example, increasing the number of components, and ensuring that the atomic size difference, for at least some of the constituents, is above 12% and that the heats of mixing among the main constituent elements are negative [12]. A number of more recent studies have identified quantities that are correlated with GFA, such as the viscosity [13], glass transition and crystallization temperatures [14,15], and atomic [16,17] and electronic [18] structure. Despite these guiding principles, we still lack a predictive understanding of BMG formation. For example, we do not even know the relative entropic and enthalpic contributions to the glass-forming ability of metal alloys, which would be a first step in computationally designing new BMGs with arbitrary compositions.

We focus on a simple model glass-forming system, bidisperse hard spheres, to quantify the entropic contribution to the glass-forming ability as a function of the atomic size ratio α, number fraction x_S of small atoms, and compression rate R (which is analogous to the cooling rate in systems with soft interaction potentials [19]). When hard-sphere systems are compressed sufficiently rapidly, they do not undergo an equilibrium freezing transition, and remain structurally disordered on the metastable branch of the equation of state. Upon further compression, hard-sphere systems jam into one of many packings with vanishing free volume at packing fraction ϕ_J, which depends on the compression rate as well as the initial condition as shown in Fig. 1(a). In the infinite compression rate limit, $\phi_J(\infty)$ approaches random close packing (with $\phi_{\rm rcp} \approx 0.64$ for monodisperse spheres [20]). In the $R \to 0$ limit, hard-sphere packings form perfect crystalline structures at $\phi_c > \phi_J$ (with face-centered-cubic symmetry and $\phi_c = \pi/\sqrt{18}$ for monodisperse spheres) [21]. At finite, but slow compression rates, "random crystals" form with many crystal defects and amorphous domains with $\phi_{\rm rcp} < \phi_J^x < \phi_c$.

We seek to determine the variables that control the critical compression rate R_c, below which crystalline domains begin to form in bidisperse hard-sphere systems as a function of
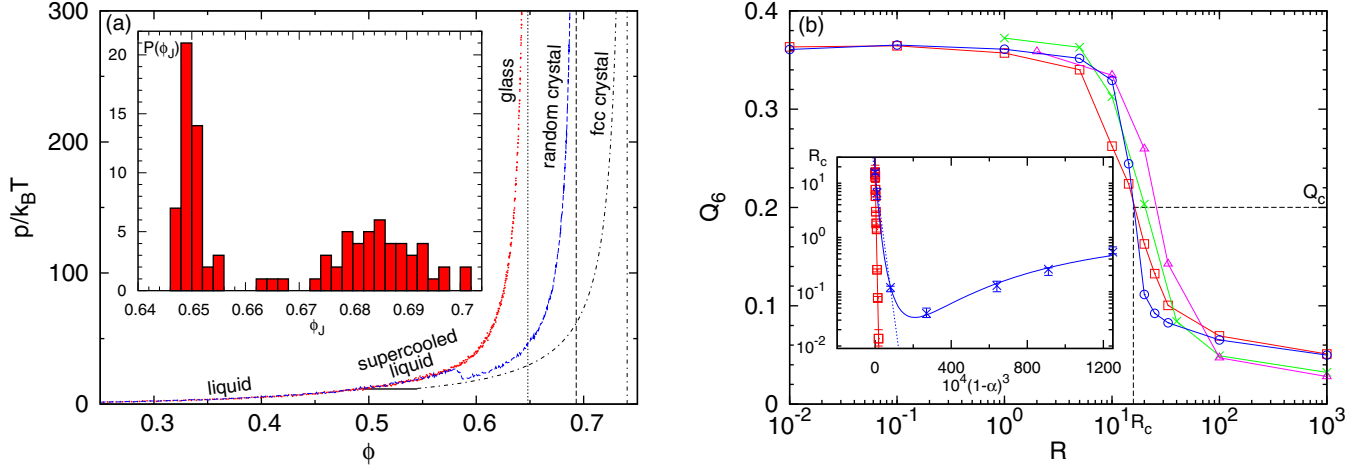
FIG. 1. (Color online) (a) Pressure $p/k_B T$ versus packing fraction ϕ for monodisperse hard spheres at compression rate $R \sim R_c \approx 10$. The dotted and dashed branches terminate at $\phi_J^a \approx 0.648$ (leftmost vertical line) and $\phi_J^x \approx 0.693$ (central vertical line), which correspond to typical disordered and "random crystal" configurations. The equilibrium $p(\phi)$ (dot-dashed line) terminates at the close-packed face-centered-cubic (fcc) crystal with $\phi_c = \pi/\sqrt{18}$ [21] (rightmost vertical line). In the inset, we show the probability distribution $P(\phi_J)$ of jammed packing fractions from 96 random initial conditions. (b) The mean (squares) and median (circles) global bond-orientational order parameter Q_6 versus R for $\alpha = 1$ and $N = 500$. The mean Q_6 for $N = 1372$ (crosses) and 2048 (triangles) are also shown. We define the critical compression rate R_c (and Q_c) by the intersection of the mean and median Q_6. In the inset, we show that for $x_S = 0.5$, R_c is monotonic over the given dynamic range and scales as $R_c \sim \exp[-C(1 - \alpha)^3]$, with $C \approx 4000$ (solid line), for $0.88 < \alpha < 1$. R_c obeys similar scaling for $x_S = 0.2$ (with $C \approx 600$; dotted line), but R_c begins to increase for $\alpha < 0.8$.

α and x_S. For example, is the packing fraction of crystalline configurations with a particular type of order important, and if so, which one at each α and x_S? Or is the packing fraction of typical amorphous configurations more important for determining the glass formability? Our computational studies show that over a wide range of size ratios and compositions where partial demixing does not occur, $R_c \sim \exp(-1/\Delta\phi_J^2)$ is controlled by the packing fraction difference $\Delta\phi_J$ between the average packing fraction of the amorphous configurations and that of the competing random crystal configurations. We find that the densest crystal structures at each α and x_S do not directly compete with glass formation. For systems with $\alpha < \alpha_c$, partial demixing intervenes and R_c has a more complex dependence on $\Delta\phi_J$. Further, we show that most known metal-metal binary bulk metallic glasses occur in the region of the α and x_S parameter space with the smallest R_c for bidisperse hard-sphere mixtures (Fig. 4), which suggests that the hard-sphere model is sufficient for explaining important general features of the GFA of metal-metal BMGs.

II. MODEL AND METHOD

We study binary mixtures of $N = N_L + N_S = 500$ hard spheres with the same mass m and diameter ratio $\alpha = \sigma_S/\sigma_L < 1$ of small to large particles using event-driven (energy-conserving) molecular dynamics (MD) simulations within a cubic box of volume V under periodic boundary conditions. We also performed simulations of monodisperse systems with $N = 1372$ and 2048 particles to investigate finite-size effects. We first prepare equilibrium liquids at a given α and small particle fraction $x_S = N_S/N$ at initial packing fraction $\phi = \frac{\pi}{6} \frac{N\sigma_L^3}{V}[1 + (\alpha^3 - 1)x_S] = 0.25 = \phi_0$. To compress the system, we increase the particle sizes by a factor

$\gamma = \min_{i<j}\{r_{ij}/\sigma_{ij}\}$, while preserving α, until the first pair of spheres comes into contact [22,23], where r_{ij} is the separation between particles i and j and $\sigma_{ij} = (\sigma_i + \sigma_j)/2$. Between each compression, the system is equilibrated at constant volume for a time interval τ, during which we measure the collision frequency and pressure. This protocol gives rise to an exponential approach to the final jammed packing fraction ϕ_J:
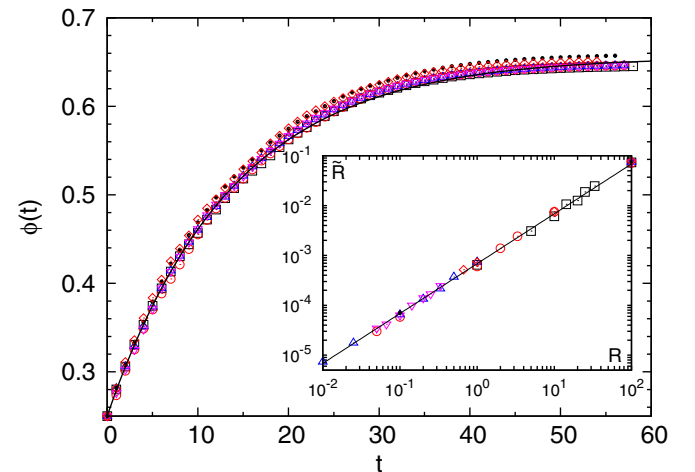

FIG. 2. (Color online) Packing fraction $\phi(t)$ versus time t for compression rate $R = 100$ for six binary hard-sphere mixtures: monodisperse systems, $\alpha = 1$ (squares), and (α, x_S) combinations, (0.9, 0.2) (open circles), (0.9,0.5) (upward triangles), (0.8, 0.2) (downward triangles), (0.7, 0.8) (filled circles), and (0.5, 0.2) (diamonds). The solid line obeys $\phi_J - \phi(t) = (\phi_J - \phi_0)e^{-\tilde{R}t}$ with $\tilde{R}$ given in the inset as a function of R. We find that $\tilde{R} = kR$ with $k \sim 7 \times 10^{-4}$. The solid line in the inset has slope 1.

$\phi_J - \phi(t) = (\phi_J - \phi_0)e^{-\tilde{R}t}$, where $\tilde{R} = kR$, k is a constant, and $R = 1/\tau$ (expressed in units of $\sqrt{k_B T/m\sigma_L^2}$, where $k_B T$ is the thermal energy) is used to vary the compression rate (Fig. 2). We terminate the hard-sphere MD compression protocol when the pressure exceeds $p/k_B T = 10^3$ at ϕ_J'. We then implemented soft-particle techniques [24] to compress the packings at $p/k_B T \sim 10^3$ to jammed packings at $p \to \infty$, $\phi_J > \phi_J'$, with $(\phi_J - \phi_J')/\phi_J' \ll 1$.

At each R, we compress 96 systems with different random initial particle positions to generate the distribution $P(\phi_J)$ of jammed packing fractions. As shown in the inset of Fig. 1(a), $P(\phi_J)$ is bimodal with a narrow peak corresponding to amorphous configurations and a broad peak corresponding to random crystal configurations. We also calculate the global bond-orientational order parameter Q_6 for each configuration [25], where nearest-neighbor particles are identified using Voronoi tessellation [26]. We find that the global bond orientational order parameter Q_6 is strongly correlated with the jammed packing fraction ϕ_J (Fig. 3). Thus we expect that the distribution $P(Q_6)$ is also bimodal for $R \sim R_c$, as shown
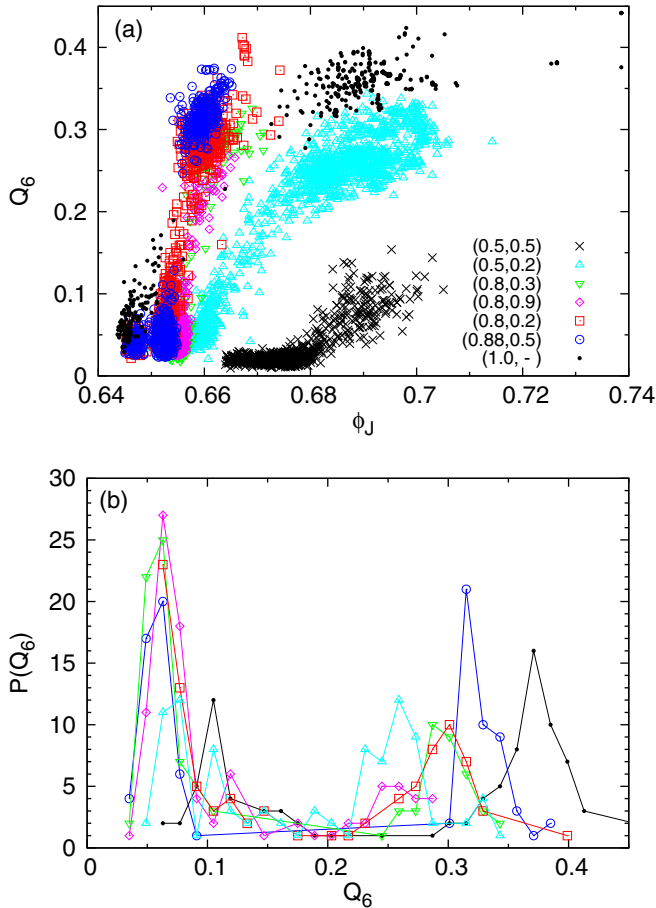
in Fig. 3, which indicates that some of the initial conditions compress to amorphous packings, while others compress to random crystals.

The relative weight of the two peaks in $P(Q_6)$ shifts toward the random crystal peak as R decreases, which causes both the mean and median Q_6 to increase. We define the critical compression rate R_c at the intersection of the mean and median Q_6 [Fig. 1(b)]. The weak system size dependence found for Q_6 versus compression rate R for $N \geqslant 500$ shown in Fig. 1(b) is consistent with the result that the critical nucleus for crystallization in monodisperse systems is fairly small (roughly 200 particles) [27]. In addition, recent computational studies have found that the critical nucleus for a binary Lennard-Jones system ($x_S = 1/3$ and $\alpha = 0.85$) is comparable to that for monodisperse systems [28].

III. RESULTS

We present extensive computational studies of the glass-forming ability for binary hard-sphere mixtures as a function of α and x_S. Our results are organized into four sections [glass-forming ability (GFA), connection between the GFA and packing efficiency, demixing, and densest crystalline packings] below.

A. Glass-forming ability

We have shown previously that for relatively large $\alpha \sim 1$, R_c decreases exponentially as

$$R_c \sim \exp[-C(1-\alpha)^3], \qquad (1)$$

where C depends on x_S [29]. As α decreases further, R_c becomes nonmonotonic, as shown in the inset to Fig. 1(b) for $x_S = 0.2$. We find that most known binary bulk metallic glass-forming alloys possess α and x_S with the smallest values of R_c for binary hard spheres. In Fig. 4, we show contour plots of R_c as a function of α and x_S for binary hard spheres. To construct the contours, we directly measured R_c (downward triangles) from MD simulations as well as employed Eq. (1) to extrapolate R_c (upward triangles) in systems where $R_c < 10^{-3}$ is below the simulation threshold. In panel (a), we identify a region bounded approximately by $0.45 \lesssim \alpha \lesssim 0.85$ and $0.35 \lesssim x_S \lesssim 0.9$, where the binary hard-sphere model predicts $R_c \lesssim 10^{-4}$. Note that for $\alpha < 0.7$, the good glass-forming regime shifts toward increasingly larger x_S. In contrast, the good glass-forming regime near $\alpha = 0.85$ includes the broadest range of x_S.

Using contours extrapolated to $R_c \sim 10^{-12}$, we find that the lowest values of R_c occur over a narrower regime between $0.73 \lesssim \alpha \lesssim 0.8$ and $0.5 \lesssim x_S \lesssim 0.8$. In particular, at $x_S = 0.5$, R_c begins to increase for $\alpha \lesssim 0.8$ due to demixing. Our previous studies of binary Lennard-Jones [29] and current studies of hard-sphere mixtures show that the composition with the smallest R_c at each α is $x_S^* = 1/(1 + \alpha^3)$ at which the large and small particles occupy the same volume. We expect that this relation will persist for $\alpha \gtrsim 0.73$. Binary metal-metal BMGs [30–32] tend to cluster near x_S^* and populate the low-R_c region of the contour plot. In contrast, binary metal-metalloid BMGs [14] do not cluster near x_S^*, possess only a small fraction
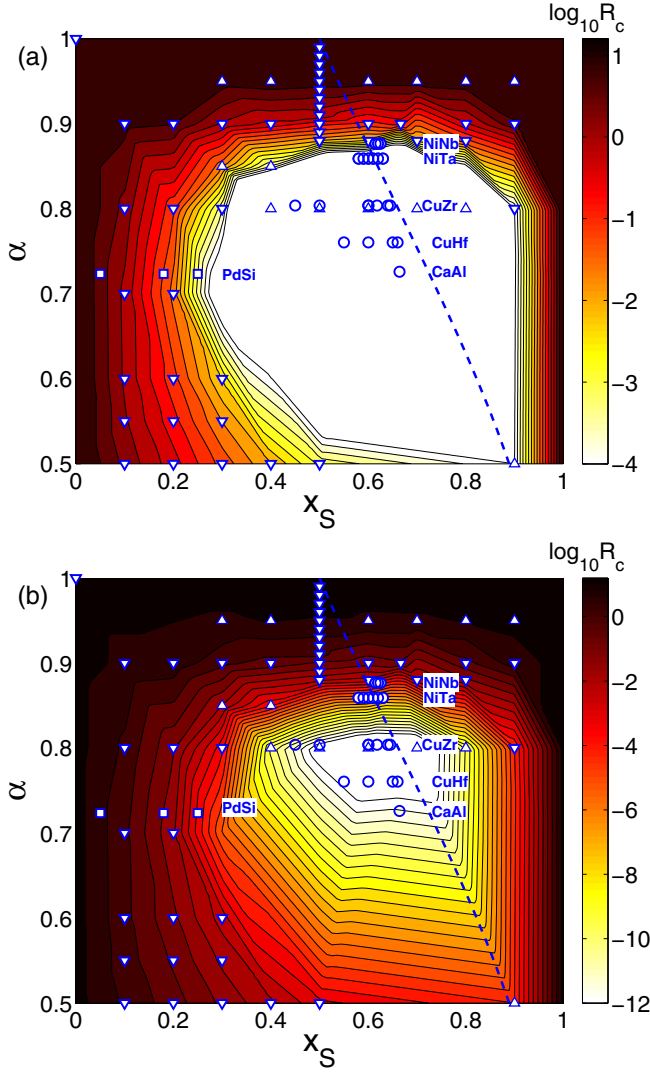

FIG. 3. (Color online) (a) Scatter plot of the global bond orientational order parameter Q_6 versus the jammed packing fraction ϕ_J for seven (α, x_S) combinations: $(1.0, -)$ (dots), $(0.5, 0.5)$ (crosses), $(0.5, 0.2)$ (upward triangles), $(0.8, 0.3)$ (downward triangles), $(0.8, 0.9)$ (diamonds), $(0.8, 0.2)$ (squares), and $(0.88, 0.5)$ (circles). (b) Probability distribution $P(Q_6)$ for the global bond orientational order Q_6 for compression rates $R \sim R_c$ for the same (α, x_S) combinations.

FIG. 4. (Color online) Contour plots of R_c versus α and x_S. The shading from dark to light indicates decreasing R_c on a (base-10) logarithmic scale. The downward triangles are from MD simulations, the upward triangles are obtained by fitting R_c to Eq. (1), and the circles and squares correspond to known metal-metal (e.g., NiNb, NiTa, CuZr, CuHf, and CaAl [30–32]) and metal-metalloid (e.g., PdSi [14]) binary BMGs, respectively. The dashed line satisfies $x_S^* = (1 + \alpha^3)^{-1}$, at which the large and small particles occupy the same volume. R_c contours in the central region are extrapolated down to $R_c \sim 10^{-4}$ (a) and 10^{-12} (b).

($\lesssim 30\%$) of small atoms, and lie outside the low-R_c region for binary hard spheres [33].

B. Connection between packing efficiency and glass-forming ability

We now seek to determine the connection between the glass-forming ability measured by R_c and packing efficiency by focusing on the mean packing fractions ϕ_J^a and ϕ_J^x of the subpopulations of amorphous and random crystal configurations, respectively, at R_c. To calculate $\langle\phi_J^a\rangle$ ($\langle\phi_J^x\rangle$), we average the packing fractions of the jammed configurations with $Q_6 < Q_c$ ($Q_6 > Q_c$). In Fig. 5(a), we plot R_c and the
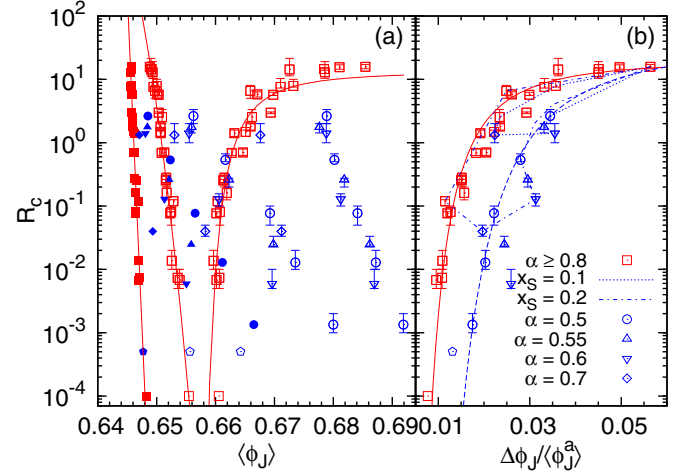

FIG. 5. (Color online) (a) R_c and the corresponding packing fractions $\langle\phi_J^a\rangle$ and $\langle\phi_J^x\rangle$ evaluated at R_c (open symbols with $\langle\phi_J^a\rangle < \langle\phi_J^x\rangle$). $\langle\phi_J^a\rangle$ for jammed packings in the $R \to \infty$ limit (filled symbols) are also shown. We compare $\langle\phi_J^a\rangle$ and $\langle\phi_J^x\rangle$ for systems with $\alpha \gtrsim 0.8$ (red squares), which remain well-mixed even after forming random crystals (i.e., polymorphic crystallization), and systems with $\alpha = 0.8$ and $x_S = 0.3$ (pentagons), as well as $\alpha = 0.7$ (diamonds), 0.6 (downward triangles), 0.55 (upward triangles), and 0.5 (circles) over a range of x_S, which partially demix before (nonpolymorphic) crystallization. (b) R_c versus packing fraction deviation $\Delta\phi_J = \langle\phi_J^x\rangle - \langle\phi_J^a\rangle$. Systems that remain well mixed (squares) collapse onto the master curve given by Eq. (3) (solid line) with $-a \approx 4 \times 10^{-4}$ and $I_\infty \approx 1.3$. We highlight systems at fixed composition, $x_S = 0.1$ (dotted line) and 0.2 (dot-dashed line), and varying α. The dashed line shows Eq. (3) with $-a \approx 10^{-3}$ and $I_\infty \approx 1.6$, which fits the R_c data for $\alpha = 0.5$. Error bars give the standard deviation over 96 initial conditions.

corresponding $\langle\phi_J^a\rangle$ and $\langle\phi_J^x\rangle$ for each α and x_S pair studied. We find that (for systems that remain well mixed) decreases in R_c are accompanied by increases in the packing efficiency of the amorphous configurations and decreases in the random crystal packing efficiency. We can identify a relation between R_c and the packing fraction deviation $\Delta\phi_J \equiv \langle\phi_J^x\rangle - \langle\phi_J^a\rangle$ by comparing R_c and the nucleation rate, I,

$$R_c \sim I = I_\infty e^{-\Delta G^*/k_B T}, \quad (2)$$

where $\Delta G^* \sim \gamma^3/\Delta\mu^2$ is the nucleation free-energy barrier, γ is the surface tension of random crystal clusters, $\Delta\mu$ is the volume contribution to the change in free energy from adding a particle to a cluster, and I_∞ is the kinetic prefactor. For hard spheres, $\Delta\mu = -k_B T \Delta S$, $\log R_c \sim 1/\Delta S^2$, and thus

$$\log R_c = a\big(\Delta\phi_J/\langle\phi_J^a\rangle\big)^{-2} + \log I_\infty, \quad (3)$$

where $a < 0$, for $\Delta\phi_J/\langle\phi_J^a\rangle \ll 1$. The thermodynamic drive for random crystal formation scales to zero with $\Delta\phi_J$, which enhances the glass formability. We show in Fig. 5(b) that Eq. (3) collapses the data for R_c for $\alpha \gtrsim 0.8$. However, for systems with $\alpha \lesssim 0.8$, the behavior of R_c is more complicated.

C. Demixing

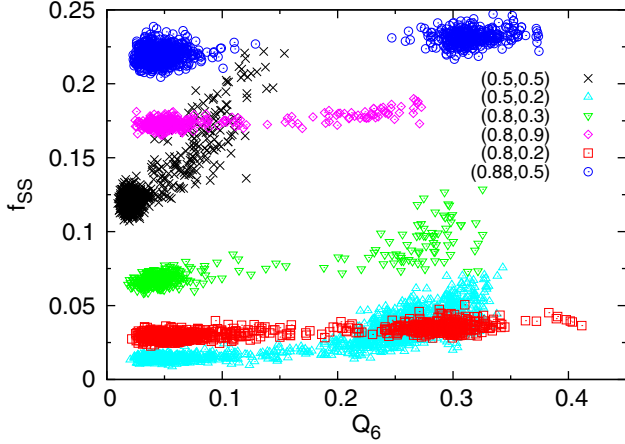In Fig. 6, we show the fraction of small-small nearest neighbors [34] as a function of Q_6 for several α and x_S pairs,

FIG. 6. (Color online) Fraction of small-small nearest neighbors f_{SS} versus Q_6 for six (α, x_S) values: $(0.5, 0.5)$ (crosses), $(0.5, 0.2)$ (upward triangles), $(0.8, 0.3)$ (downward triangles), $(0.8, 0.9)$ (diamonds), $(0.8, 0.2)$ (squares), and $(0.88, 0.5)$ (circles). f_{SS} for $(0.8, 0.9)$ has been shifted downward by 0.6 to enable comparison with the other systems. The systems with $(0.5, 0.5)$, $(0.5, 0.2)$, and $(0.8, 0.3)$ partially demix as indicated by the increase in f_{SS} with increasing Q_6.

where nearest-neighbor particles share Voronoi-polyhedra faces. We find that systems with $\alpha \lesssim 0.8$ exhibit partial demixing prior to the formation of random crystals (i.e., nonpolymorphic crystallization) as evidenced by the increase in f_{SS} with increasing Q_6. In Fig. 7(a), we show the evolution of the small particle radial distribution function $g_{SS}(r)$ with increasing packing fraction during compression of a system with $\alpha = 0.5$ and $x_S = 0.5$ at $R < R_c$. The strong increase in the second peak in $g_{SS}(r)$ at $r/\sigma_L \sim 1$ for $\phi > 0.59$ is a signature of demixing (i.e., the clustering of small particles and clustering of large particles into separate groups). We also studied the time evolution of the demixing process after compression to a fixed packing fraction $\phi = 0.59$. In Fig. 7(b), we show that the fraction of contact types f_{SS} and f_{LL} increase strongly (and f_{SL} decreases) near time $t = 4 \times 10^4$ for the same system in panel (a), which indicates strong demixing. Initially, the small and large particles are well mixed. As time progresses, the small particles move through the interstices formed by the large particles, while the large particles are relatively less mobile. At long times, the large particles are clustered together surrounding pockets of trapped small particles.

For systems with small size ratios, e.g., $\alpha = 0.5$, the large particles form the rigid backbone of the random crystal, while the small particles, which can fit in the interstices of the large-particle backbone, remain disordered. We find that demixing encourages the formation of random crystals, which results in lower R_c at the same $\Delta\phi_J$ compared to systems that remain well mixed. Even though there is more scatter for the systems that partially demix, R_c decreases strongly with decreasing $\Delta\phi_J$ as x_S is varied at fixed α. At fixed composition (e.g., $x_S = 0.1$ or 0.2), R_c versus $\Delta\phi_J$ deviates from the $\alpha \gtrsim 0.8$ master curve as α decreases below 0.8, but it eventually reconnects with the monodisperse systems for sufficiently small α.
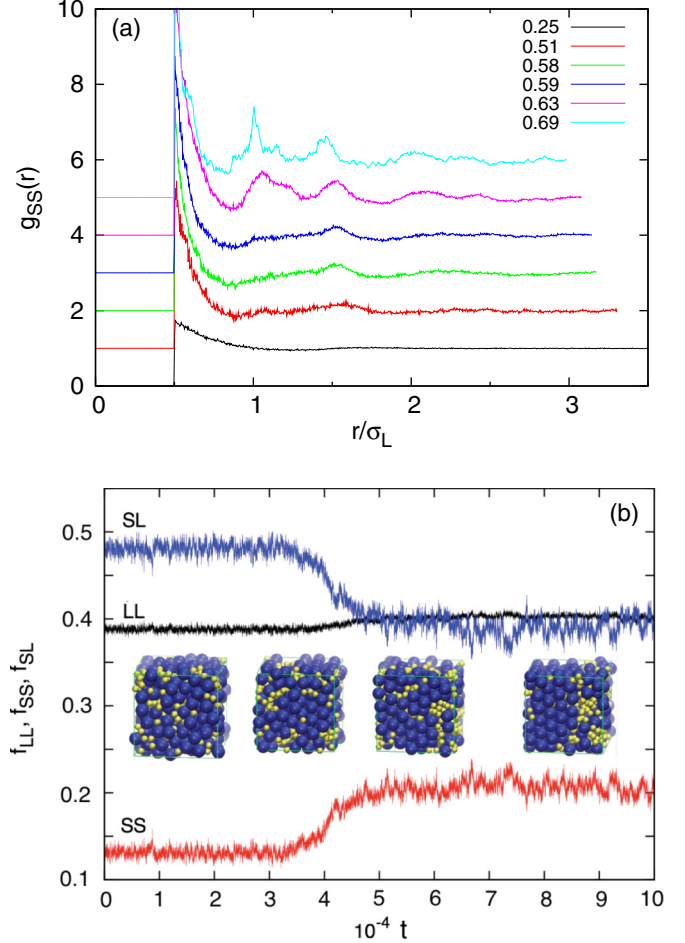

FIG. 7. (Color online) (a) Radial distribution function $g_{SS}(r)$ of small particles in binary mixtures of size ratio $\alpha = 0.5$ and small particle number fraction $x_S = 0.5$ at various packing fractions ($\phi = 0.25$, 0.51, 0.58, 0.59, 0.63, and 0.69 from bottom to top) at compression rate $R = 10^{-3} < R_c$. (b) Small-small f_{SS}, large-large f_{LL}, and small-large f_{SL} particle contact fraction versus time t for the same system in panel (a) compressed to $\phi = 0.59$. The inset shows configurations at $t = 0, 4 \times 10^4$, 5×10^4, and 10^5 (from left to right) as the system begins to demix.

Structural differences between the well-mixed and demixed systems can also be found in the disordered configurations in the $R \to \infty$ limit. For example, $\langle \phi_J^a \rangle$ obtained from jammed packings in the $R \to \infty$ limit is strongly correlated with R_c for the well-mixed systems; however, the data is highly scattered for the demixed systems. By analyzing the radial distribution function $g(r)$, we find that the structural symmetry between the small and large particles does not occur for $\alpha \lesssim 0.8$. Instead, the large particles form the rigid backbone of the jammed packing, while the peaks in $g(r)$ corresponding to separations between small particles broaden and become liquidlike, as shown in Fig. 8.

D. Densest crystalline packings

We implemented a genetic optimization algorithm [35] to identify the densest binary packings of hard spheres as a function of the size ratio α and small particle composition x_S.
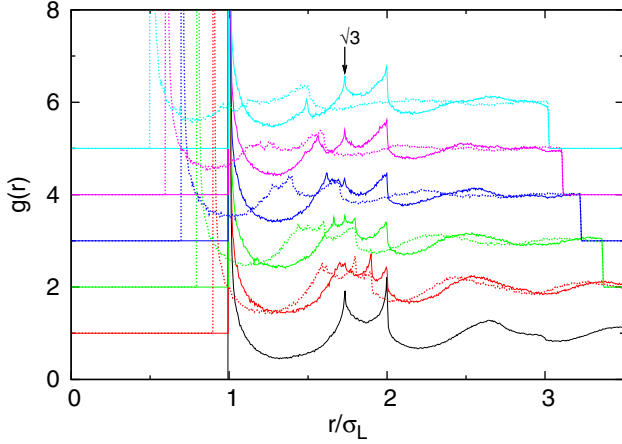
FIG. 8. (Color online) Radial distribution function $g(r)$ versus separation r (normalized by the large particle diameter σ_L) between large-large (solid lines) and small-small (dotted lines) particle pairs for size ratios $\alpha = 0.5, 0.6, 0.7, 0.8, 0.9,$ and 1.0 (from top to bottom) at fixed $x_S = 0.5$. For $\alpha < 0.8$, $g(r)$ for the small-small and large-large pairs are no longer strongly coupled.

As shown in Fig. 9(a), neither the least nor the most efficient packing regimes correlate well with the best glass-forming regime shown in Fig. 4. In particular, at $\alpha = 0.5$ and $x_S = 2/3$, we find that the AB_2 compound with $\phi = 0.758$ [Fig. 9(b)] has the highest packing fraction in the α-x_S plane. However, in this region of the α-x_S plane, hard-sphere systems are susceptible to demixing at finite compression rates, not formation of dense AB_2 crystals. For the compression rates we consider in this work, it is the random crystal (not the densest crystal) that competes with glass formation and determines the GFA. The emergence of the less thermodynamically stable random crystal can be understood using Ostwald's step rule [36]. Although the AB_2 crystal is most stable, its nucleation rate is much smaller than that of random fcc crystals [37]. The AB_2 nucleation rate has a small kinetic prefactor I_∞, which is proportional to the inverse time that it takes a single A particle to "pair" with two B particles.

IV. CONCLUSIONS

There have been few theoretical and computational studies that have quantified the GFA for binary and ternary hard-sphere systems and identified which particular values of α and x_S yield the best glass formers. In this work, we have shown that the binary hard-sphere model explains several general features of the GFA for metal-metal BMGs. First, the densest crystal structures do not directly determine the GFA. In particular, for systems with $\alpha \gtrsim 0.8$ that do not demix, $R_c \sim \exp(-1/\Delta\phi_J^2)$ is set by the average packing fraction deviation $\Delta\phi_J$ between the amorphous and *random* crystal configurations, and $R_c \to 0$ as $\Delta\phi_J$ tends to zero. For systems with $\alpha \lesssim 0.8$ that partially demix, each $R_c(\alpha)$ obeys a similar curve. In addition, most known metal-metal BMGs occur in the low-R_c region of α and x_S parameter space for binary hard spheres, but metal-metalloid BMGs do not. Our studies show that maximizing the glass-forming ability in binary
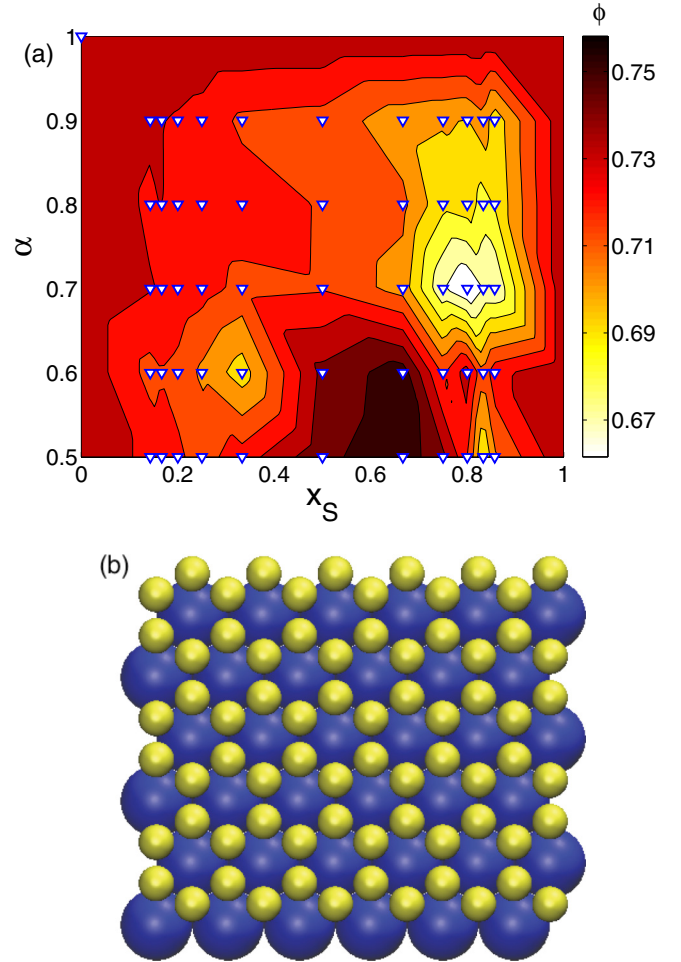

FIG. 9. (Color online) (a) Packing fraction ϕ of the densest crystal packings (triangles) of bidisperse hard spheres as a function of size ratio α and small particle composition x_S obtained using a genetic optimization algorithm [35]. The contours interpolate between the data points. (b) AB_2 compound with $\phi = 0.758$ obtained from the genetic algorithm at size ratio $\alpha = 0.5$ and small particle composition $x_S = 2/3$.

systems involves competing effects: minimizing α to increase packing efficiency and maximizing α to reduce the tendency for demixing. This suggests that the GFA can be increased in ternary systems by preventing demixing. These results can be tested experimentally in colloidal glasses and BMGs using novel combinatorial design techniques [38].

[1] M. Leocmach and H. Tanaka, Nat. Commun. **3**, 974 (2012).

[2] J.-P. Hansen and I. R. McDonald, *Theory of Simple Liquids* (Academic Press, London, 1986).

[3] C. Song, P. Wang, and H. A. Makse, Nature (London) **453**, 629 (2008).

[4] J. D. Weeks, D. Chandler, and H. C. Andersen, J. Chem. Phys. **54**, 5237 (1971).

[5] D. B. Miracle, Nat. Mater. **3**, 697 (2004).

[6] H. L. Peng, M. Z. Li, W. H. Wang, C.-Z. Wang, and K. M. Ho, Appl. Phys. Lett. **96**, 021901 (2010).

[7] A. Inoue, Acta Mater. **48**, 279 (2000).

[8] W. H. Wang, C. Dong, and C. H. Shek, Mater. Sci. Eng. R **44**, 45 (2004).

[9] C. A. Schuh, T. C. Hufnagel, and U. Rammurty, Acta Mater. **55**, 4067 (2007).

[10] J. Schroers, Phys. Today **66**(2), 32 (2013).

[11] W. H. Wang, Prog. Mater. Sci. **52**, 540 (2007).

[12] A. Inoue, T. Zhang, and A. Takeuchi, Mater. Sci. Forum **269–272**, 855 (1998).

[13] N. Wang, L. Ji, W. J. Yao, and Y. P. Zheng, J. Appl. Phys. **111**, 103525 (2012).

[14] Z. P. Lu and C. T. Liu, Acta Mater. **50**, 3501 (2002).

[15] X. H. Du, J. C. Huang, C. T. Liu, and Z. P. Lu, J. Appl. Phys. **101**, 086108 (2007).

[16] D. B. Miracle and D. V. Louzguine-Luzgin, Mater. Rev. **55**, 218 (2010).

[17] Y. Q. Cheng, E. Ma, and H. W. Sheng, Phys. Rev. Lett. **102**, 245501 (2009).

[18] H. B. Yu, W. H. Wang, and H. Y. Bai, Appl. Phys. Lett. **96**, 081902 (2010).

[19] R. Kurita and E. R. Weeks, Phys. Rev. E **82**, 041402 (2010).

[20] M. D. Rintoul and S. Torquato, Phys. Rev. Lett. **77**, 4198 (1996).

[21] R. Hoste and W. van Dael, J. Chem. Soc., Faraday Trans. 2 **80**, 477 (1984).

[22] P. Jalali and M. Li, Intermetallics **12**, 1167 (2004).

[23] P. Jalali and M. Li, Phys. Rev. B **71**, 014206 (2005).

[24] G.-J. Gao, J. Blawzdziewicz, and C. S. O'Hern, Phys. Rev. E **74**, 061304 (2006).

[25] P. J. Steinhardt, D. R. Nelson, and M. Ronchetti, Phys. Rev. B **28**, 784 (1983).

[26] H. W. Sheng, W. K. Luo, F. M. Alamgier, J. M. Bai, and E. Ma, Nature (London) **439**, 419 (2006).

[27] S. Auer and D. Frenkel, Nature (London) **409**, 1020 (2001).

[28] S. Jungblut and C. Dellago, J. Chem. Phys. **134**, 104501 (2011).

[29] K. Zhang, M. Wang, S. Papanikolaou, Y. Liu, J. Schroers, M. D. Shattuck, and C. S. O'Hern, J. Chem. Phys. **139**, 124503 (2013).

[30] D. Xu, B. Lohwongwatana, G. Duan, W. L. Johnson, and C. Garland, Acta Mater. **52**, 2621 (2004).

[31] L. Xia, W. H. Li, S. S. Fang, B. C. Wei, and Y. D. Dong, J. Appl. Phys. **99**, 026103 (2006).

[32] Y. Wang, Q. Wang, J. Zhao, and C. Dong, Scr. Mater. **63**, 178 (2010).

[33] P. F. Guan, T. Fujita, A. Hirata, Y. H. Liu, and M. W. Chen, Phys. Rev. Lett. **108**, 175501 (2012).

[34] C. F. Schreck, C. S. O'Hern, and L. E. Silbert, Phys. Rev. E **84**, 011305 (2011).

[35] L. Filion and M. Dijkstra, Phys. Rev. E **79**, 046714 (2009).

[36] W. Ostwald, Z. Phys. Chem. **22**, 289 (1897).

[37] P. R. ten Wolde and D. Frenkel, Phys. Chem. Chem. Phys. **1**, 2191 (1999).

[38] S. Ding, Y. Liu, Y. Li, S. Sohn, F. J. Walker, and J. Schroers, Nat. Mater. **13**, 494 (2014).